ACS OMEGA

Article

Cite This: ACS Omega 2019, 4, 4296−4303

http://pubs.acs.org/journal/acsodf

Enhanced Forward Osmosis Desalination with a Hybrid Ionic Liquid/Hydrogel Thermoresponsive Draw Agent System

Chih-Hao Hsu,[†] Canghai Ma,[†] Ngoc Bui,[†] Zhuonan Song,[†] Aaron D. Wilson,[‡] Robert Kostecki,[§] Kyle M. Diederichsen,[∥] Bryan D. McCloskey,[∥] and Jeffrey J. Urban*[,†]

[†]The Molecular Foundry and [§]Energy Storage and Distributed Resources Division, Lawrence Berkeley National Laboratory, Berkeley, California 94720, United States

[‡]Idaho National Laboratory, P.O. Box 1625 MS 2208, Idaho Falls, Idaho 83415, United States

[∥]Department of Chemical and Biomolecular Engineering, University of California, Berkeley, Berkeley, California 94720, United States

Supporting Information

ABSTRACT: Forward osmosis (FO) has emerged as a new technology for desalination and exhibits potentials for applications where reverse osmosis is incapable or uneconomical for treating streams with high salinity or fouling propensity. However, most of current draw agents in FO are salts and difficult to be recycled cost- and energy-effectively. In this work, we demonstrate a new and facile approach to efficiently recover water from the FO process with enhanced water purity by using a binary ion liquid/hydrogel system. The hybrid ion liquid/hydrogel draw solution system demonstrated in this work synergistically leverages the thermoresponsive properties of both the ionic liquid (IL) and hydrogel to improve the overall FO performance. Our findings corroborate that the hydrogel mitigates the water flux decline of the IL as the draw agent and provide a ready route to contiguously and effectively regenerate water from the FO process. Such a route allows for an efficient recovery of water from the draw solute/water mixture with enhanced water purity, compared with conventional thermal treating of lower critical solution temperature IL draw solute/water. Furthermore, hydrogels can be used in a continuous and readily recyclable process to recover water without heating the entire draw solute/water mixture. Our design principles open the door to use low-grade/waste heat or solar energy to regenerate draw agents and potentially reduce energy in the FO process considerably.

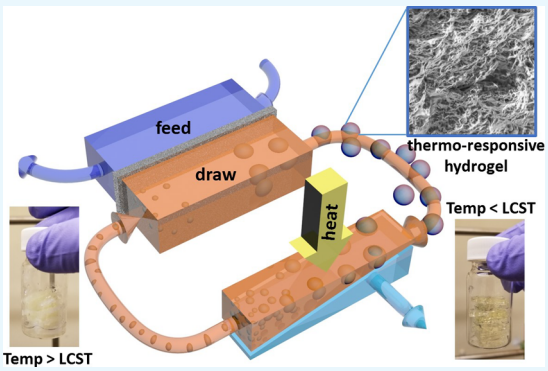

INTRODUCTION

The rising global demand for unconventional water resources due to rapid population expansion, urban development, industrialization, and climate change has urged global scientists to multidirectionally leverage first-principles scientific innovations toward a future of sustainable water and energy.[1,2] Oftentimes, the critical challenge lies at the codependent relationship between water and energy. In essence, early-stage innovative technologies need to couple energy frameworks into the big picture. For desalination, the current leading technology is reverse osmosis (RO), a pressure-driven membrane-based separation process where water is allowed to pass through a semipermeable membrane that rejects salts. With the advent of technologies in high-performance membranes, energy recovery devices, and efficient pumps, seawater RO (SWRO) now consumes much less energy than thermal desalination and has been the benchmark for any new desalination technology.[3] Still, SWRO plants consume 3−4 times the theoretical minimum energy for desalination because of the need of extensive pre- and post-treatment processes.[3] Furthermore, being highly dependent on thermoelectric energy as the main power source, SWRO inevitably creates a non-negligible carbon footprint which further exacerbates climate change and intensifies the ecological imbalance.

To augment freshwater sources, any low-quality water sources should be considered. For local areas where access to a cumbersome SWRO plant is impossible, a mobile and compact system that can be flexibly plugged in at the point-of-use and does not require high-grade energy is a must, that is, when emerging technologies such as solar-assisted portable systems (e.g., solar humidification/dehumidification desalination, solar pond, and solar still), membrane distillation, (electro)adsorption, and forward osmosis (FO) come into play, each of which has its own pros and cons.[4,5] Being spontaneously driven by a chemical potential (i.e., osmotic pressure difference) created by two solutions with different

Received: October 15, 2018
Accepted: January 4, 2019
Published: February 27, 2019

DOI: 10.1021/acsomega.8b02827
ACS Omega 2019, 4, 4296−4303

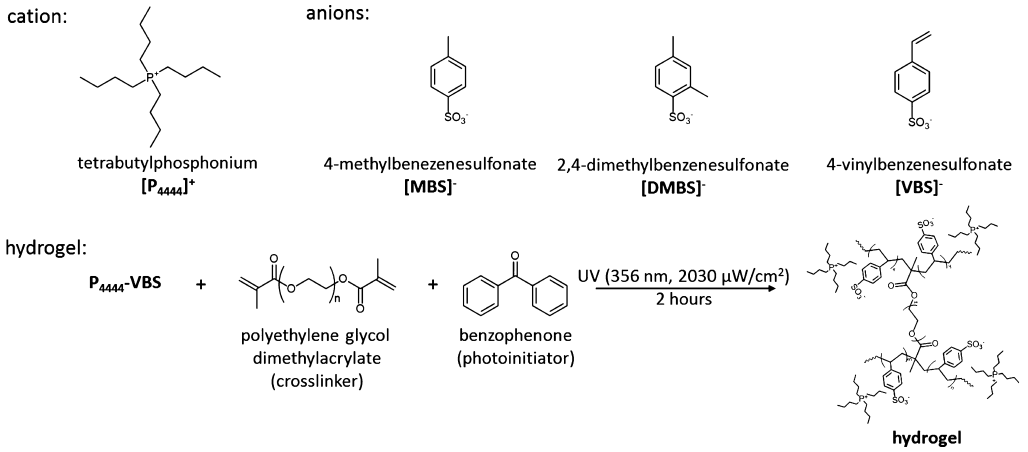

Figure 1. Chemical structures of ILs and the synthetic route of the thermoresponsive hydrogel.

salinities across a semipermeable membrane, FO is considered as a potentially viable energy-efficient desalination technology[6] with low fouling propensity.[7,8] Sharing the same modularity potential as RO but with a capability of desalinating water with a low-grade or waste heat source, FO is thus attractive to niche point-of-use water applications where no/low-pressure operation and infrequent membrane replacement are required. Furthermore, FO can be readily integrated with other post-treatment stages such as nanofiltration,[9] ultrafiltration,[10] membrane distillation,[11,12] or low-pressure RO[13] when need be.[14] Especially, in such a hybrid system, if solar energy can be effectively integrated with the FO module, total electricity consumption for the whole process will be predominantly determined by the post-treatment step.

With FO, however, one of the energy-intensive steps is to regenerate the osmotic agent (or draw solute), a critical factor that once improved might help enhance the practicality and applicability for FO. Easy separation/recycle must therefore be considered as an important criterion for an ideal draw solute besides others such as high osmotic strength, non-toxicity, and low cost. Besides conventional inorganic solutes, several approaches for stable and regenerable draw agents with high osmotic potential have been proposed in recent years,[15] such as organic solutes (e.g., switchable polarity solvents[16]), surface-modified nanomaterials (e.g., magnetic nanoparticles),[17,18] hybrid organic−inorganic multivalent salts (e.g., phosphazene[19]), or polyelectrolytes.[20,21] Although rendering draw agent systems with remarkably high osmotic potential and regenerability, these systems still encounter difficulties related to (1) (ir)reversible agglomeration (for nanomaterials which require further costs to redisperse them back into the solutions to maintain high osmotic strength upon reusing), (2) solvent-induced membrane degradation (for switchable polarity solvent systems which require high-cost solvent-resistant membranes), (3) pumping energy intensiveness (for polyelectrolyte systems because of their high viscosity), or (4) the need for energy-inefficient phase-separating and trace-removal steps to recover draw solutes such as CO_2-assisted phase separation and/or reverse osmosis.[22]

To enable an energy-efficient separation of draw solutes from water for (1) collection of uncontaminated freshwater and (2) regeneration of draw solutes, leveraging solar thermal energy and/or industrial low-grade heat as the energy source is inevitable.[23] Thermoresponsive materials are thus attractive for draw solutes to help realize this target.[12,24−27] Among those, ionic liquids (ILs) stand out as prominent candidates as their ionic nature generally guarantees a high osmotic pressure. Unlike commonly used inorganic salts in FO, the chemical structure of both cations and anions of ILs can be readily fine-tuned to exhibit desired thermodynamic properties.[28,29] More specifically, for the FO process, well-designed ILs undergo a lower critical solution temperature (LCST) phase transition which significantly decreases its miscibility with water upon heating.[30−32] As this phase transition of IL/water mixtures can occur at relatively low temperature (∼50 °C), IL-derived draw solutes can function effectively in a solar-powered FO desalination process and so does the cross-linked versions of LCST ILs, that is, hydrogels, as they retain the LCST phase behavior in this form.[33−38]

When thermoresponsive upper critical solution temperature or LCST ILs are used as draw solutes for FO, their regeneration typically involve two phases: water-rich and IL-rich phase.[29] The IL-rich phase can be recirculated back to FO to replenish the draw solution, whereas the water-rich phase needs a further filtration step, for example, nanofiltration, to produce fresh water. The water-rich phase, although has a substantially lower solute concentration than sea/brackish water, still contains ∼10 wt % of ILs according to the lever rule of their U-shape LCST phase diagram (see the Results and Discussion section for details). To recover water from IL-derived draw solutes with much less solutes, hydrogels appear to be more beneficial as they are cross-linked ILs. However, these hydrogels are often directly immobilized into FO membranes[34,35,39] and thus markedly limit their integration into a continuous FO process. To synergistically leverage the advantages offered by ILs and hydrogels while overcoming each of their drawbacks, we deterministically tailor a binary draw solute system incorporating both thermoresponsive ILs and hydrogels and study their behaviors in the FO process. The feasibility of using the hydrogel to mitigate the water flux decline of the IL draw and recycling water from the hydrogel is specifically demonstrated in this study. The overarching goal is to render a draw solute system that can effectively function in a continuous FO process, providing fresh water with minimal solute contamination and requiring minimal electrical energy for regeneration.[40,41]

RESULTS AND DISCUSSION

To have ILs with a LCST phase behavior, a subtle balance between hydrophilicity and hydrophobicity is required for the

DOI: 10.1021/acsomega.8b02827
ACS Omega 2019, 4, 4296−4303

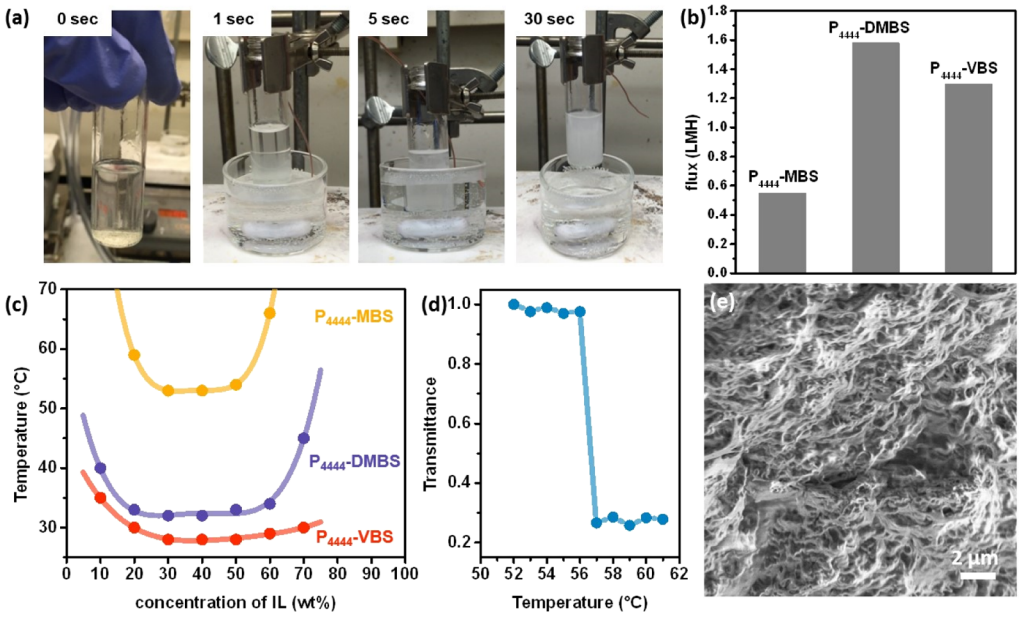

Figure 2. (a) Observation of the LCST phase transition in a 10 wt % P_{4444}−VBS solution at 50 °C for varying time periods. (b) Draw ability of 10 wt % IL solution as DSs against DI water as the FS. The FO test was conducted with 50 g of draw and feed solutions as the initial condition at 25 °C. (c) LCST phase diagram of ILs at varying concentrations. The temperatures were determined by the turbidity curves with an experimental error <1 °C. (d) Temperature-dependent turbidity curves of the hydrogel (λ = 600 nm). (e) SEM image of the freeze-dried hydrogel.

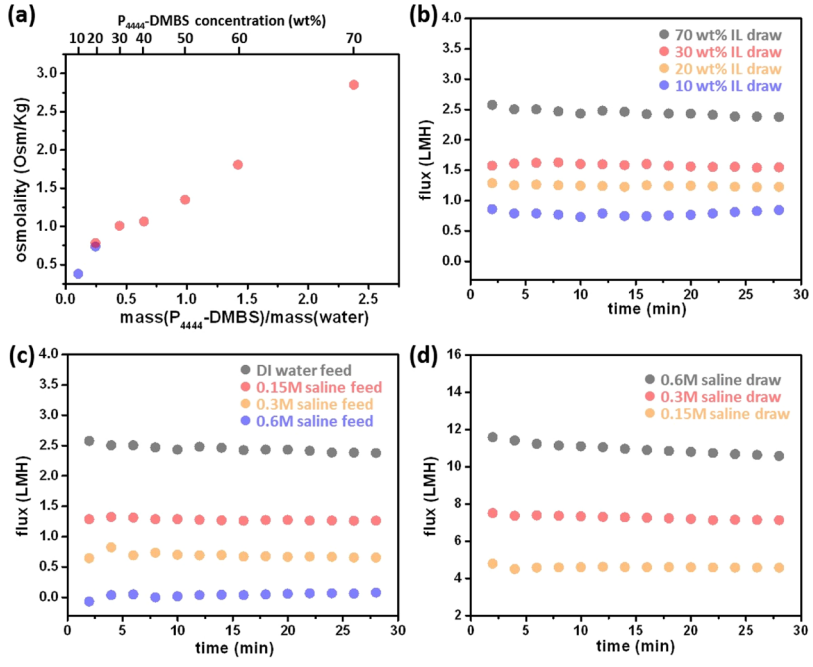

Figure 3. (a) Osmolality of P_{4444}−DMBS solutions measured by the freezing point method (blue) and vapor pressure method (red). Water flux profiles of (b) P_{4444}−DMBS with varying concentrations as DSs against DI water as the FS, (c) 70 wt % P_{4444}−DMBS as the DS against saline water at various concentrations as FSs, and (d) saline water with varying concentrations as DSs against DI water. The FO measurements were conducted with Aquaporin-inside membranes at 25 °C.

ionic components.[29,31] In this study, we focused on ILs with tetrabutyl phosphonium ($[P_{4444}]^+$) as the cation because of its balanced amphiphilicity and capability to show LCST with a variety of anions. Three different anions, including 4-methylbenzensulfonate ($[MBS]^-$), 2,4-dimethylbenzensulfonate ($[DMBS]^-$), and 4-vinylbenzenesulfonate ($[VBS]^-$) anions (Figure 1), were assessed in terms of phase-transition temperature and draw ability for FO. Note that P_{4444}−VBS was assessed not only as a draw solute but also as a monomer for hydrogels by cross-linking the vinyl groups (Figure 1). The phase separation occurs immediately (<5 s) after heating above its LCST, as shown for 10 wt % P_{4444}−VBS at 50 °C (Figure 2a). To understand the dependence of IL concentration on the phase separation temperature, IL/water mixtures with varying concentrations were measured by temperature-dependent UV−vis spectroscopy to generate the corresponding turbidity curves (Figure S1). The drop of transmittance at λ = 600 nm was used to interpret the LCST for each IL/water mixture.

DOI: 10.1021/acsomega.8b02827
ACS Omega 2019, 4, 4296−4303

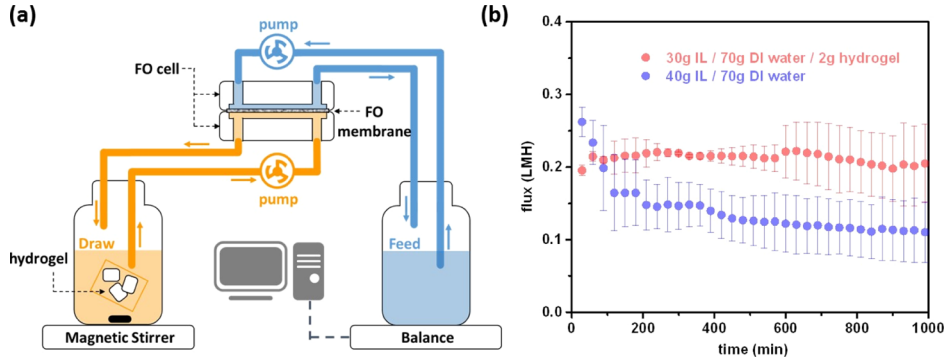

Figure 4. (a) Schematic illustration of the FO setup. (b) Long-term FO experiments with various draw compositions against 0.15 M saline water feed, showing that the synergistic effect of incorporating the hydrogel with ILs retains the draw ability in the long run. The FO measurements of 30 g P_{4444}–DMBS/2 g hydrogel and 40 g P_{4444}–DMBS DSs were conducted with cellulose triacetate (CTA) membranes. The reverse IL flux is 13.6 ± 2.7 g/m^2·h (0.031 ± 0.006 mol/m^2·h) in our IL/hydrogel binary draw system-of-interest.

The dependence of concentration on the transmittance drop temperature is summarized in an LCST phase diagram (Figure 2c). Among the three ILs, P_{4444}–MBS exhibits the highest transition temperature across the entire concentration range, whereas P_{4444}–DMBS shows a moderate LCST behavior with a transition temperature of 33 °C at 50 wt % and P_{4444}–VBS shows the lowest with LCST of 28 °C at 50 wt %. The draw ability of ILs was initially assessed by using 10 wt % ILs as draw solutions (DSs) against deionized water (DI) as the feed solution (FS) (Figure 2b). Because P_{4444}–DMBS possesses the highest draw ability and a moderate LCST phase behavior, we focus on evaluating the potential of P_{4444}–DMBS as the IL draw solute in the binary system.

The turbidity curve of the hydrogel was measured with the swollen hydrogel (twice of its original weight) (Figure 2d). Because the hydrogel mainly consists of P_{4444}–VBS, the LCST of the swollen hydrogel is expected to be close to the LCST of 50 wt % P_{4444}–VBS, that is, 30 °C (Figure 2c). Counter-intuitively, a LCST phase transition was detected at 56 °C for the hydrogel (Figure 2d). We hypothesized that this interesting shift in LCST was perhaps due to the addition of poly(ethylene oxide) as a flexible cross-linker which then plasticized the IL structural network. The scanning electron microscopy (SEM) image of the freeze-dried water-contained hydrogel clearly shows the sponge-like structure (Figure 2e), confirming its capability of absorbing water.

The viscosity (Figure S3) and osmolality of P_{4444}–DMBS were further assessed as a function of concentration. The osmotic concentration relative to the mass ratio of IL and water (Figure 3a) does not generally follow mole stoichiometric trends.[42] The IL behaves as a near-ideal solute[43] at dilute conditions until a cluster-forming domain begins, which results in a plateau of the osmotic pressure as increase in concentration beyond that point is involved in cluster formation. Beyond this cluster-forming regime, there is then a rise in osmotic pressure as the bulk water between clusters is removed at higher concentrations. A similar trend has been observed in other solutes[44] including LCST materials.[45] Osmotic water flux was measured in the FO mode (active layer faced the DS) to evaluate P_{4444}–DMBS as a draw solute against DI water and saline water FS (Figure 3b,c). Direct FO measurement of 70 wt % P_{4444}–DMBS against saline water FS with varying salinities shows an intriguing insight into the draw ability of P_{4444}–DMBS. Specifically, the 70 wt % IL solution is able to extract water from 0.15 to 0.3 M saline water (Figure 3c). Although the water flux we observed for 70 wt % P_{4444}–DMBS against DI water is lower than that of using a common draw solute, such as NaCl (Figure 3d), these results have shown a similar and even higher flux compared to using other ILs as the draw solute[27] and possess other advantages.

The synergistic effect created when both IL and hydrogel were used as draw solutes was evaluated with the setup shown in Figure 4a. Hydrogels packaged in a tea bag were placed in the DS bottle. The micrometer size pore of the tea bag allows an unhindered flow of the IL solution while preventing hydrogels from flowing into tubes and clogging the FO cell. The DS was stirred continuously throughout the whole FO process to ensure a well-mixing and homogeneous solution, and the weight change of the FS was recorded digitally and converted into water flux (see Material and Experiment section for details). The contrast of using solely IL and an IL/hydrogel binary system as draw solutes is clearly shown in Figure 4b. Because the initial flux (J_{ini}) is dominated by the IL concentration, J_{ini} obtained by the 40 g IL draw solute (J_{ini} = 0.26 L·m^{-2}·h^{-1}) was higher than that of the 30 g IL/2 g hydrogel draw solute (J_{ini} = 0.19 L·m^{-2}·h^{-1}). However, the flux performed by the former case decreased significantly more rapidly than the latter case because of the loss of osmotic pressure by continuous dilution. Furthermore, the 30 g IL/2 g hydrogel performed even better than the 40 g IL in the long run (>100 min). This enhanced durability of the binary draw system is contributed to the relatively constant IL concentration in the DS. In a tandem fashion, hydrogels are able to simultaneously extract water from the IL solution which then allows IL to draw water from the FS at a relatively constant draw ability. Noticeably, because the monomer of hydrogels is almost chemically identical to the IL, using 30 g IL/2 g hydrogel in 70 g of DI water is equivalent to 31.4 wt % IL in terms of the amount of active materials, which is lower than the case of using 40 g IL in 70 g of DI water (36.4 wt %). This means that the binary draw solute system can not only reduce the cost of draw solutes but also reinforce the draw performance in a long run while maintaining a comparably low reverse solute flux, of 13.6 ± 2.7 g/m^2·h (or 0.031 ± 0.006 mol/m^2·h) (Figure S4) as those performed by typical IL-based draw solute systems reported in the literature.[46,47] Note that these values were compared when cellulose acetate membranes were used for FO tests.

As aforementioned, the water in hydrogels can then be retrieved by a thermal treatment. To evaluate this capability,

DOI: 10.1021/acsomega.8b02827
ACS Omega 2019, 4, 4296−4303

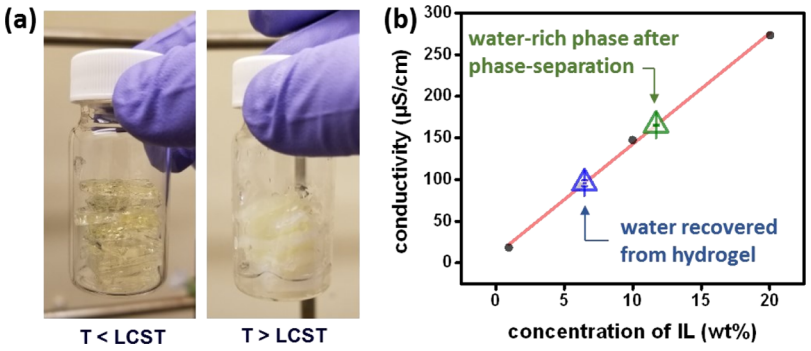

Figure 5. (a) Procedure of water recovery from hydrogels. (b) IL/water conductivity calibration curve and recycled water conductivity (all samples were diluted by 89 times): $y = 13.308x + 8.9607$ ($R^2 = 0.9986$).

after the FO experiment, the water-saturated hydrogel exhibited a weight of 5.8 g, suggesting that a significant amount of water (1.9 times of the initial hydrogel weight) was adsorbed by the hydrogel. The hydrogel was further heated at 60 °C to recover the water from the hydrogel system (Figure 5a). In this process, the hydrogel sample was first loaded in a sealed syringe and then heated in a water bath at 60 °C upon which an amount of liquid emerged within a few minutes. To calculate the water content emerging from this step of regenerating the hydrogel while collecting fresh water, a calibration curve of P_{4444}–DMBS/water mixtures was first created. Briefly, samples with 1, 6, 10, and 20 wt % of P_{4444}–DMBS were prepared and diluted by 89 times by adding desired amounts of DI water. Conductivity was measured on the diluted samples, which exhibited a strong linear correlation with $R^2 = 0.9986$, as depicted in Figure 5b. Likewise, the liquid sample from the hydrogel was diluted using the same ratio as being used in the calibration (i.e., 89 times) and then measured with a conductivity probe. The recycled liquid displayed a conductivity of 93 μS/cm, which corresponds to an amount of only 6 wt % IL (blue triangle in Figure 5b). A reasonably high purity of water could thus be recovered from the process (of 94 wt % in this study). Because P_{4444}–DMBS has been demonstrated to exhibit very low cytotoxicity by using human fibroblast cell models,[30] traces of ILs in the output stream do not necessarily need be treated for some applications, for example, thermoelectric power plant cooling. For the purpose of producing drinking water, the output stream can be further treated by the nanofiltration process, and the LCST behavior of P_{4444}–DMBS provides an opportunity to utilize thermal energy in the secondary process.

To probe the effectiveness of using a hydrogel to recover water from the ion liquid versus directly heating the ion liquid, a 30 wt % P_{4444}–DMBS solution was also heated at 60 °C to phase-separate water from the system using the same thermal treatment for regenerating the swollen hydrogel. As expected, the homogenous ion liquid/water mixture started to show two phases (water-rich phase on top and IL-rich phase at bottom) when heating it up to a temperature higher than the phase change temperature of 56 °C. The water-rich phase from the top solution was again diluted by 89 times and showed a conductivity of 165 μS/cm, suggesting a content of 12 wt % IL (green triangle in Figure 5b). We estimated that the water content from heating the IL/water mixture was only 88 wt %, relatively lower than the 94 wt % in the case with the hydrogel. We believe that directly heating the hydrogel affords another facile and effective approach to recover water from the draw solution with a high water purity and efficiency without the need of heating the entire draw solute, potentially providing significant reduction of energy for water regeneration for the FO process.

CONCLUSIONS

In this study, a proof-of-concept regarding leveraging ILs both in their natural and cross-linked (hydrogel) forms for use as a binary draw solute system for FO is shown. Three thermoresponsive ILs and a hydrogel with similar chemical identity have been assessed as the draw solutes for FO, and the corresponding LCST phase behavior was studied with UV–vis spectroscopy. With the considerations of osmotic strength and phase transition temperatures, P_{4444}–DMBS was used in a binary draw system with hydrogels. The synergistic effect of using the IL/hydrogel binary draw solute system has been demonstrated in terms of (1) creating a more durable DS with less active materials, (2) the water recovered from the hydrogel contains less solutes compared to direct phase separation of IL solutions, and (3) the hydrogels are in a mobile phase which makes a continuous FO process possible. In all, the proposed binary IL/hydrogel solute system, in its infancy, shows encouraging results toward a future of a sustainably and energy-efficiently solar-driven FO process where just a small portion of the DS, that is hydrogel, needs to go through a simple replenishing process to retrieve fresh water with decent purity. Further improvement of FO performance in this approach is expected by coupling hydrogels with other draw solutes with high osmotic strength, for example, inorganic salts or organic salts.

MATERIALS AND EXPERIMENTS

Materials. Tetra-*N*-butylphosphonium chloride (>80% in water), sodium 2,4-dimethylbenzenesulfonate monohydrate (>98%), sodium 4-vinylbenzenesulfonate (>93%), and sodium *p*-toluenesulfonate were purchased from VWR. Dichloromethane (HPLC grade), poly(ethylene glycol) dimethacrylate (average M_n = 550 Da), and benzophenone (reagentplus, 99%) were purchased from Sigma-Aldrich. All chemicals were used in synthesis without further purification. DI water used in this study was produced by the Milli-Q system (Advantage, A10).

Characterization. ^{1}H NMR spectra were recorded in $CDCl_3$ on a Bruker AVANCE III NMR spectrometer (500 MHz) at room temperature. For the SEM characterization, a piece of the swollen hydrogel (twice of its original weight) was freeze-dried by the lyophilizer (LABCONCO, FreeZone 4.5 Plus) overnight and then coated with a thin Au layer. The SEM image was recorded on a Zeiss Gemini Ultra-55 Analytical

DOI: 10.1021/acsomega.8b02827
ACS Omega 2019, 4, 4296–4303

Field Emission SEM system. The LCSTs of ILs and the hydrogel were determined by monitoring the transmittance of light (λ = 600 nm, ASD QualitySpec Pro UV−vis spectrometer). A temperature-controlled water reservoir was coupled to the UV−vis cuvette, and the temperature of the IL solution was directly recorded by a thermocouple in situ (Figure S1a). Viscosity was measured using an electromagnetically spinning viscometer (EMS-1000, Kyoto Instruments). This technique measures viscosity based on the rotation rate and magnetically applied force to a 2 mm aluminum ball located in the testing solution. The viscometer was calibrated using known standards (Cannon Instruments Inc.) and was within 3% of the known values. Temperature was maintained at 25 °C throughout the measurement, a rotation rate of 1000 rpm was used, and the reported values represent the average of at least 10 individual viscosity measurements on the same solution (Figure S3a). Additional viscosity measurements were made using the falling bob method at 15 °C with a Cambridge Applied Systems VL4100 viscometer (Figure S3b). Inductively coupled plasma-optical emission spectrometry (ICP-OES) test, performed on Varian ICP-OES 720 Series, was used to quantify the total trace amount (ppm to ppb) of ILs crossing over the membrane from the draw to the feed during FO tests. After FO tests, samples of the feed was collected and diluted by 100 times before ICP tests. Phosphorous 1000 ppm standard solution (Sigma-Aldrich) was used to prepare diluted standard solutions having phosphorus concentration ranging from 0.1 to 250 ppm. Osmotic pressures of low concentration of IL aqueous solutions (i.e., 10 and 20 wt %) were measured by freezing point depression osmometry using an Advanced Instruments Inc. model 3250 Osmometer. Osmotic pressures of high concentration of IL aqueous solutions were converted by the water activity (eqs 1 and 2) measured via non-contact resistive electrolytic sensor technology on a Novasina LabMaster Standard Water Activity Instrument (range −0.003 to 1.00a_w, with an accuracy of ±0.003a_w) with Full Temperature Control (0−50 °C, with an accuracy of ±0.3 °C).

$$a_w = p/p_0 \quad (1)$$

$$-\ln(a_w)/V_m \approx \text{Osm/kg} \quad (2)$$

Synthesis of ILs and the Hydrogel. P_{4444}−MBS was prepared by dissolving tetra-*N*-butylphosphonium chloride (10 g, 27 mmol) and sodium *p*-toluenesulfonate (5.35 g, 27 mmol) in DI water (25 mL) and stirring overnight. The dissolved mixture was extracted by dichloromethane (20 mL for three times) and then washed by DI water (10 mL for three times). The solvent was removed by rotary evaporation at 80 °C. ^{1}H NMR (500 MHz, $CDCl_3$): δ 0.89−0.93 (t, 12H, CH_3), 1.35−1.43 (m, 16H, CH_2), 2.01−2.16 (m, 8H, CH_2), 2.22 (s, 3H, CH_3), 6.94−7.06 (d, 2H, CH), 7.56−7.68 (d, 2H, CH) ppm (Figure S2a).

P_{4444}−DMBS was prepared by dissolving tetra-*N*-butylphosphonium chloride (100 g, 270 mmol) and sodium 2,4-dimethylbenzene sulfonate monohydrate (56.5 g, 270 mmol) in DI water (275 mL) and stirring overnight. The dissolved mixture was extracted by dichloromethane (20 mL for three times) and then washed by DI water (10 mL for three times). The solvent was removed by rotary evaporation at 80 °C. ^{1}H NMR (500 MHz, $CDCl_3$): δ 0.89−0.93 (t, 12H, CH_3), 1.35−1.43 (m, 16H, CH_2), 1.98−2.07 (m, 8H, CH_2), 2.26 (s, 3H, CH_3), 2.60 (s, 3H, CH_3), 6.96 (d, 1H, CH), 6.99 (s, 1H, CH), 7.78 (d, 1H, CH) ppm (Figure S2b).

P_{4444}−VBS was prepared by dissolving tetra-*N*-butylphosphonium chloride (50 g, 135 mmol) and sodium 4-vinylbenzenesulfonate (30.9 g, 135 mmol) in DI water (175 mL) and stirring overnight. The dissolved mixture was extracted by dichloromethane (20 mL for three times) and then washed by DI water (10 mL for three times). The solvent was removed by rotary evaporation at 60 °C. ^{1}H NMR (500 MHz, $CDCl_3$): δ 0.89−0.93 (t, 12H, CH_3), 1.43−1.45 (m, 16H, CH_2), 2.23−2.25 (m, 8H, CH_2), 5.19−5.22 (d, 1H, CH), 5.69−5.73 (d, 1H, CH), 6.63−6.68 (q, 1H, CH), 7.26−7.34 (d, 2H, CH), 7.81−7.83 (d, 2H, CH) ppm (Figure S2c).

The hydrogel was prepared by mixing P_{4444}−VBS (2 g), poly(ethylene glycol) dimethacrylate (50 mg), and benzophenone (8.24 mg) under nitrogen followed by 2 h of UV-curing (356 nm, 2030 μW/cm^2, Spectrolinker XL-1500 Series UV Crosslinker).

FO Measurement. Commercial flat sheet membranes were used in this study, including Aquaporin-inside FO membranes (Sterlitech) and CTA flat sheet membranes (HTI). The Aquaporin-inside membrane was soaked in DI water for 1 h to replace the liquid in the package before use, and the CTA membrane was stored in a 2% Na_2SO_3 solution and rinsed with DI water before use. A commercial membrane cell (Sterlitech, CFO42A) was used for the FO measurements to sandwich the flat-sheet membranes with a total membrane active area of 42 cm^2. In the FO measurement, the active layer of FO membrane faced the draw solution (AL−DS configuration). The general FO experimental procedure started with 100 g of FS and 100 g of DS in the glass media bottles. For the study of the synergistic effect of the binary draw solute system, 30g and 40 g ILs (P_{4444}−DMBS) were dissolved in 70 g of DI water, separately, and an additional 2 g of hydrogel in a tea bag was placed in the 30 g IL solution. In this way, the draw performance of 30 g IL + 2 g hydrogel can be directly compared with 40 g IL. A gear pump (LongerPump, BT 100-1L) was used to continuously recirculate both DS and FS at a flow rate of 120 mL·min^{-1}. A stirrer was used in the DS bottle to ensure good mixing of DS and water extracted from FS. The mass variation of DS was monitored by a digital balance (Veritas) with a uncertainty of ± 5 mg and converted to the permeate flux. The first 15 min of each batch was used to stabilize the system, and then, the flux was calculated from the proceeding time and mass loss of the FS reservoir.

Water Regeneration from the IL/Water Mixture. In this work, when the water permeation data was completed, the hydrogel was removed from the IL mixture with the external surface quickly cleaned with paper towels and was weighted to record the water trapped in the hydrogel. Afterward, the hydrogel was placed in a syringe and heated at a 60 °C water bath, and the water started to phase-separate from the swollen hydrogel. The syringe was only used for draining the phase-separated water phase and no pressure was applied on the hydrogel. A freshly synthesized hydrogel (2 g) was studied, which yielded a limited quantity of liquid samples of 3.3 g. For the conductivity measurement (Oakton cond 6+), the liquid sample was diluted by 89 times by DI water. To estimate the water content in the sample from regeneration, a calibration curve was created by preparing IL/water mixtures with known IL content from 1 to 20 wt % and subsequently diluted by 89 times using DI water to ensure consistency with the calibration sample with recycled water. Conductivity was measured on the diluted samples and plotted into a calibration curve.

DOI: 10.1021/acsomega.8b02827
ACS Omega 2019, 4, 4296−4303

■ ASSOCIATED CONTENT

Supporting Information

The Supporting Information is available free of charge on the ACS Publications website at DOI: 10.1021/acsomega.8b02827.

UV−vis setup for measuring the phase transition temperature of the IL solution and corresponding turbidity curves of three ILs; ^{1}H NMR spectra of three ILs; viscosity data of P_{4444}−DMBS; and reverse solute flux performed by our binary draw system-of-interest (PDF)

■ AUTHOR INFORMATION

Corresponding Author

*E-mail: jjurban@lbl.gov (J.J.U.).

ORCID

Kyle M. Diederichsen: 0000-0002-6787-7996
Bryan D. McCloskey: 0000-0001-6599-2336
Jeffrey J. Urban: 0000-0002-6520-830X

Author Contributions

C.-H.H. designed the experiments, synthesized the materials, and wrote the manuscript. C.M. and Z.S. carried out the FO measurements and data interpretation. C.M., N.B., and R.K. wrote the manuscript and provided insights for experimental design. N.B. measured the trace amount of ILs in the feed with ICP-OES. A.D.W. measured the osmolality and viscosity data. K.M.D. and B.D.M. measured the viscosity data. J.J.U. supervised the project and contributed to experimental design and interpretation.

Notes

The authors declare no competing financial interest.

■ ACKNOWLEDGMENTS

This work was supported by the Molecular Foundry, Laboratory Directed Research and Development (LDRD) Program, and the Assistant Secretary for Energy Efficiency and Renewable Energy, Geothermal Technologies Office of the US Department of Energy under the USDOE contract number DE-AC02-05CH11231 for Lawrence Berkeley National Laboratory. We would like to thank Dr. Baoxia Mi for providing the CTA FO membranes and Dr. Fen Qiu for her help in performing SEM characterization.

■ REFERENCES

(1) Urban, J. J. Emerging Scientific and Engineering Opportunities within the Water-Energy Nexus. *Joule* **2017**, *1*, 665−688.

(2) Shannon, M. A.; Bohn, P. W.; Elimelech, M.; Georgiadis, J. G.; Mariñas, B. J.; Mayes, A. M. Science and technology for water purification in the coming decades. *Nature* **2008**, *452*, 301−310.

(3) Elimelech, M.; Phillip, W. A. The Future of Seawater Desalination: Energy, Technology, and the Environment. *Science* **2011**, *333*, 712−717.

(4) Li, C.; Goswami, Y.; Stefanakos, E. Solar assisted sea water desalination: A review. *Renewable Sustainable Energy Rev.* **2013**, *19*, 136−163.

(5) Chandrashekara, M.; Yadav, A. Water desalination system using solar heat: A review. *Renewable Sustainable Energy Rev.* **2017**, *67*, 1308−1330.

(6) Klaysom, C.; Cath, T. Y.; Depuydt, T.; Vankelecom, I. F. J. Forward and pressure retarded osmosis: potential solutions for global challenges in energy and water supply. *Chem. Soc. Rev.* **2013**, *42*, 6959−6989.

(7) Achilli, A.; Cath, T. Y.; Marchand, E. A.; Childress, A. E. The forward osmosis membrane bioreactor: A low fouling alternative to MBR processes. *Desalination* **2009**, *239*, 10−21.

(8) Zhao, S.; Zou, L.; Tang, C. Y.; Mulcahy, D. Recent developments in forward osmosis: Opportunities and challenges. *J. Membr. Sci.* **2012**, *396*, 1−21.

(9) Tan, C. H.; Ng, H. Y. A novel hybrid forward osmosis - nanofiltration (FO-NF) process for seawater desalination: Draw solution selection and system configuration. *Desalin. Water Treat.* **2010**, *13*, 356−361.

(10) Ling, M. M.; Chung, T.-S. Desalination process using super hydrophilic nanoparticles via forward osmosis integrated with ultrafiltration regeneration. *Desalination* **2011**, *278*, 194−202.

(11) Wang, K. Y.; Teoh, M. M.; Nugroho, A.; Chung, T.-S. Integrated forward osmosis−membrane distillation (FO−MD) hybrid system for the concentration of protein solutions. *Chem. Eng. Sci.* **2011**, *66*, 2421−2430.

(12) Zhao, D.; Wang, P.; Zhao, Q.; Chen, N.; Lu, X. Thermoresponsive copolymer-based draw solution for seawater desalination in a combined process of forward osmosis and membrane distillation. *Desalination* **2014**, *348*, 26−32.

(13) Yangali-Quintanilla, V.; Li, Z.; Valladares, R.; Li, Q.; Amy, G. Indirect desalination of Red Sea water with forward osmosis and low pressure reverse osmosis for water reuse. *Desalination* **2011**, *280*, 160−166.

(14) Chekli, L.; Phuntsho, S.; Kim, J. E.; Kim, J.; Choi, J. Y.; Choi, J.-S.; Kim, S.; Kim, J. H.; Hong, S.; Sohn, J.; Shon, H. K. A comprehensive review of hybrid forward osmosis systems: Performance, applications and future prospects. *J. Membr. Sci.* **2016**, *497*, 430−449.

(15) Zhao, D.; Chen, S.; Guo, C. X.; Zhao, Q.; Lu, X. Multi-functional forward osmosis draw solutes for seawater desalination. *Chin. J. Chem. Eng.* **2016**, *24*, 23−30.

(16) Stone, M. L.; Rae, C.; Stewart, F. F.; Wilson, A. D. Switchable polarity solvents as draw solutes for forward osmosis. *Desalination* **2013**, *312*, 124−129.

(17) Ling, M. M.; Chung, T.-S.; Lu, X. Facile synthesis of thermosensitive magnetic nanoparticles as "smart" draw solutes in forward osmosis. *Chem. Commun.* **2011**, *47*, 10788−10790.

(18) Na, Y.; Yang, S.; Lee, S. Evaluation of citrate-coated magnetic nanoparticles as draw solute for forward osmosis. *Desalination* **2014**, *347*, 34−42.

(19) Stone, M. L.; Wilson, A. D.; Harrup, M. K.; Stewart, F. F. An initial study of hexavalent phosphazene salts as draw solutes in forward osmosis. *Desalination* **2013**, *312*, 130−136.

(20) Ge, Q.; Su, J.; Amy, G. L.; Chung, T.-S. Exploration of polyelectrolytes as draw solutes in forward osmosis processes. *Water Res.* **2012**, *46*, 1318−1326.

(21) Kim, J.-j.; Kang, H.; Choi, Y.-S.; Yu, Y. A.; Lee, J.-C. Thermo-responsive oligomeric poly(tetrabutylphosphonium styrenesulfonate)s as draw solutes for forward osmosis (FO) applications. *Desalination* **2016**, *381*, 84−94.

(22) McCutcheon, J.; Bui, N. Forward Osmosis. In *Desalination: Water from Water*; Kucera, J., Ed.; John Wiley & Sons, 2014; pp 262−265.

(23) U.S. Department of Energy. *The Water-Energy Nexus: Challenges and Opportunities*; U.S. Department of Energy, 2014.

(24) Fan, X.; Liu, H.; Gao, Y.; Zou, Z.; Craig, V. S. J.; Zhang, G.; Liu, G. Forward-Osmosis Desalination with Poly(Ionic Liquid) Hydrogels as Smart Draw Agents. *Adv. Mater.* **2016**, *28*, 4156−4161.

(25) Deguchi, Y.; Kohno, Y.; Ohno, H. Design of Ionic Liquid-Derived Polyelectrolyte Gels Toward Reversible Water Absorption/Desorption System Driven by Small Temperature Change. *Aust. J. Chem.* **2014**, *67*, 1666−1670.

(26) Wan, J.; Tao, T.; Zhang, Y.; Liang, X.; Zhou, A.; Zhu, C. Phosphate adsorption on novel hydrogel beads with interpenetrating network (IPN) structure in aqueous solutions: kinetics, isotherms and regeneration. *RSC Adv.* **2016**, *6*, 23233−23241.

DOI: 10.1021/acsomega.8b02827
ACS Omega 2019, 4, 4296−4303

(27) Zhong, Y.; Feng, X.; Chen, W.; Wang, X.; Huang, K.-W.; Gnanou, Y.; Lai, Z. Using UCST Ionic Liquid as a Draw Solute in Forward Osmosis to Treat High-Salinity Water. *Environ. Sci. Technol.* **2015**, *50*, 1039−1045.
(28) Zhang, S.; Sun, N.; He, X.; Lu, X.; Zhang, X. Physical Properties of Ionic Liquids: Database and Evaluation. *J. Phys. Chem. Ref. Data* **2006**, *35*, 1475−1517.
(29) Qiao, Y.; Ma, W.; Theyssen, N.; Chen, C.; Hou, Z. Temperature-Responsive Ionic Liquids: Fundamental Behaviors and Catalytic Applications. *Chem. Rev.* **2017**, *117*, 6881−6928.
(30) Cai, Y.; Shen, W.; Wei, J.; Chong, T. H.; Wang, R.; Krantz, W. B.; Fane, A. G.; Hu, X. Energy-efficient desalination by forward osmosis using responsive ionic liquid draw solutes. *Environ. Sci.: Water Res. Technol.* **2015**, *1*, 341−347.
(31) Fukumoto, K.; Ohno, H. LCST-type phase changes of a mixture of water and ionic liquids derived from amino acids. *Angew. Chem., Int. Ed.* **2007**, *46*, 1852−1855.
(32) Kohno, Y.; Ohno, H. Temperature-responsive ionic liquid/water interfaces: relation between hydrophilicity of ions and dynamic phase change. *Phys. Chem. Chem. Phys.* **2012**, *14*, 5063−5070.
(33) Li, D.; Zhang, X.; Yao, J.; Simon, G. P.; Wang, H. Stimuli-responsive polymer hydrogels as a new class of draw agent for forward osmosis desalination. *Chem. Commun.* **2011**, *47*, 1710−1712.
(34) Li, D.; Zhang, X.; Simon, G. P.; Wang, H. Forward osmosis desalination using polymer hydrogels as a draw agent: Influence of draw agent, feed solution and membrane on process performance. *Water Res.* **2013**, *47*, 209−215.
(35) Li, D.; Zhang, X.; Yao, J.; Zeng, Y.; Simon, G. P.; Wang, H. Composite polymer hydrogels as draw agents in forward osmosis and solar dewatering. *Soft Matter* **2011**, *7*, 10048−10056.
(36) Ali, W.; Gebert, B.; Hennecke, T.; Graf, K.; Ulbricht, M.; Gutmann, J. S. Design of Thermally Responsive Polymeric Hydrogels for Brackish Water Desalination: Effect of Architecture on Swelling, Deswelling, and Salt Rejection. *ACS Appl. Mater. Interfaces* **2015**, *7*, 15696−15706.
(37) Zhang, K.; Feng, X.; Ye, C.; Hempenius, M. A.; Vancso, G. J. Hydrogels with a Memory: Dual-Responsive, Organometallic Poly(ionic liquid)s with Hysteretic Volume-Phase Transition. *J. Am. Chem. Soc.* **2017**, *139*, 10029−10035.
(38) Cai, Y.; Wang, R.; Krantz, W. B.; Fane, A. G.; Hu, X. M. Exploration of using thermally responsive polyionic liquid hydrogels as draw agents in forward osmosis. *RSC Adv.* **2015**, *5*, 97143−97150.
(39) Hartanto, Y.; Yun, S.; Jin, B.; Dai, S. Functionalized thermo-responsive microgels for high performance forward osmosis desalination. *Water Res.* **2015**, *70*, 385−393.
(40) Ge, Q.; Ling, M.; Chung, T.-S. Draw solutions for forward osmosis processes: Developments, challenges, and prospects for the future. *J. Membr. Sci.* **2013**, *442*, 225−237.
(41) Cai, Y.; Hu, X. M. A critical review on draw solutes development for forward osmosis. *Desalination* **2016**, *391*, 16−29.
(42) Wilson, A. D.; Stewart, F. F. Deriving osmotic pressures of draw solutes used in osmotically driven membrane processes. *J. Membr. Sci.* **2013**, *431*, 205−211.
(43) Lewis, G. N. The osmotic pressure of concentrated solutions, and the laws of the perfect solution. *J. Am. Chem. Soc.* **1908**, *30*, 668−683.
(44) Wilson, A. D.; Orme, C. J. Concentration dependent speciation and mass transport properties of switchable polarity solvents. *RSC Adv.* **2015**, *5*, 7740−7751.
(45) Nakayama, D.; Mok, Y.; Noh, M.; Park, J.; Kang, S.; Lee, Y. Lower critical solution temperature (LCST) phase separation of glycol ethers for forward osmotic control. *Phys. Chem. Chem. Phys.* **2014**, *16*, 5319−5325.
(46) Park, J.; Joo, H.; Noh, M.; Namkoong, Y.; Lee, S.; Jung, K. H.; Ahn, H. R.; Kim, S.; Lee, J.-C.; Yoon, J. H.; Lee, Y. Systematic structure control of ammonium iodide salts as feasible UCST-type forward osmosis draw solutes for the treatment of wastewater. *J. Mater. Chem. A* **2018**, *6*, 1255−1265.
(47) Ju, C.; Kang, H. Zwitterionic polymers showing upper critical solution temperature behavior as draw solutes for forward osmosis. *RSC Adv.* **2017**, *7*, 56426−56432.

DOI: 10.1021/acsomega.8b02827
ACS Omega 2019, 4, 4296−4303